Supporting Information for "Toward a Better Understanding of Wildfire Behavior in the Wildland-Urban Interface: A Case Study of the 2021 Marshall Fire"

Timothy W. Juliano[1], Neil Lareau[2], Maria E. Frediani[1], Kasra Shamsaei[2], Masih Eghdami[1], Karen Kosiba[3], Joshua Wurman[3], Amy DeCastro[1], Branko Kosović[1], Hamed Ebrahimian[2]

[1]Research Applications Laboratory, National Center for Atmospheric Research

[2]University of Nevada, Reno

[3]University of Illinois at Urbana–Champaign, Champaign, Illinois

Contents of this file

1. Text S1-S4
2. Figures S1 to S7

S1: WRF model setup In our two domain configuration, the outer and inner domains are resolved using a horizontal grid cell spacing of $\Delta x = \Delta y = 1000$ m and 111.11 m, respectively. We use a total of 45 model grid cells in the vertical column and set the grid cell spacing, $\Delta z \approx 25$ m adjacent to the surface before stretching with increasing height. In the outer domain, we activate the Yonsei University (YSU) planetary boundary layer

(PBL) parameterization (Hong et al., 2006) to handle vertical turbulent mixing, and 2D horizontal diffusion is computed by Smagorinsky (1963). In the inner domain, we turn off the PBL scheme and use WRF's large-eddy simulation capability by activating the three-dimensional turbulent kinetic energy (TKE)-based sub-grid scale (SGS) model of Deardorff (1980). Details about the resolved TKE calculation is described in Text S4.

S2: Marshall Fire ignition approach The first ignition, initially reported by a 911 call at 18:08 UTC, was slightly northeast of the intersection of Marshall Road and Highway-93 (approximate location: 39.956127°N, 105.230487°W). The 911 call indicated that a structure was burning uncontrollably in the intense winds. At 19:00 UTC, a Boulder park ranger on the scene noticed a second ignition location to the southwest, near the Marshall Mesa Trailhead parking lot (approximate location: 39.951209°N, 105.231441°W). This ignition occurred in dry, fine fuels and began spreading rapidly toward the northeast. In the WRF-Fire simulations, we ignite these two sources according to the above information.

Other ignitions also occurred later during the Marshall Fire likely due to ember spotting. Without any conclusive information, we hypothesize that ember spotting is the only plausible way that the fire was able to "hop" across Highway-36. Therefore, we use the firebrand spotting parameterization (Frediani et al., 2021) in WRF-Fire to produce spotting likelihood maps. We first run a simulation with only the two aforementioned primary ignitions and allow the fire to approach Highway-36. At this stage, the fire is not able to propagate further because any roadways in the fuel model are considered non-burnable fuel. However, we use the spotting parameterization to estimate where and when new ignitions are most likely to occur. While this approach is somewhat subjective, we believe

that it is reasonable, especially because the modeled fire spread appears realistic in the fine fuels. Technical details about the WRF-Fire spotting parameterization may be found in Appendix A of the WRF User Guide starting in v4.4 (`https://www2.mmm.ucar.edu/wrf/users/docs/user_guide_v4/v4.4/users_guide_chap-fire.html#firebrand`).

Two additional fire ignition locations and times, based on the spotting parameterization, are estimated: (39.9638°N, 105.180°W) at 19:40 UTC and (39.966248°N, 105.185050°W) at 20:30 UTC. We then conduct a second WRF-Fire simulation with these additional spotting ignitions and present the results in the main manuscript.

S3: Fr calculation The dimensionless Fr, which is often used to examine atmospheric flow adjustment, may be interpreted as the ratio of the mean planetary boundary layer (PBL) wind speed to the fastest possible gravity wave traveling along the fluid interface between the PBL and free troposphere. For the Fr analysis, we follow a similar approach as in (Juliano et al., 2017). Here the PBL height is determined based on the sharpest vertical gradient in the potential temperature field. Reduced gravity is computed as $g^{'} = g\frac{\theta_t - \overline{\theta_{PBL}}}{\overline{\theta_{PBL}}}$ where θ_t is the free troposphere potential temperature, $\overline{\theta_{PBL}}$ is the mean PBL potential temperature (and so $\theta_t - \overline{\theta_{PBL}}$ represents the change in θ across the PBL inversion). For θ_t, we use the θ value from two grid cells above the defined PBL top. The Fr is then calculated as $Fr = \frac{V}{\sqrt{g^{'}H}}$ where H is the PBL depth and V is the mean PBL wind speed.

S4: TKE calculation In this study, we use the TKE field to better understand the presence of a hydraulic jump (i.e., supercritical to subcritical flow transition). To compute the resolved TKE from the WRF output, we follow steps outlined in previous studies (e.g.,

Schmidli, 2013; Wagner et al., 2014). First, we decompose a fully turbulent variable, ϕ, into its model grid cell average (represented by the instantaneous model output), $\overline{\phi}$, and unresolved, $\phi^{'}$, components:

$$\phi(x,y,z,t) = \overline{\phi}(x,y,z,t) + \phi^{'}(x,y,z,t)$$

where (x,y,z,t) represents the space and time dimensions. The unresolved component is computed by the large-eddy simulation SGS model and output at each (x,y,z) grid cell and time stamp (1 min sampling interval). The resolved turbulent component, $\phi^{''}$, is then calculated as

$$\phi^{''}(x,y,z,t) = \overline{\phi}(x,y,z,t) - \langle\overline{\phi}(x,y,z,t)\rangle$$

where $\langle\ \rangle$ represents a temporal average defined as

$$\langle\ \rangle = \frac{1}{T}\int_{t-T/2}^{t+T/2} \overline{\phi}(x,y,z,t)\,dt$$

with T representing the time-averaging interval. We choose $T = 40$ min with a 1 min sampling interval, which is similar to other studies (e.g., Juliano et al., 2017, 2022). Results are relatively insensitive when using $T = 20$ min with a 1 min sampling interval (not shown).

References

Deardorff, J. W. (1980). Stratocumulus-capped mixed layers derived from a three-dimensional model. Bound.-Layer Meteor., *18*, 495–527.

Frediani, M., Juliano, T. W., DeCastro, A., Kosović, B., & Knievel, J. (2021). A fire-spotting parameterization coupled with the wrf-fire model. *Earth and Space Science Open Archive*, 12. doi: 10.1002/essoar.10506771.1

Hong, S.-Y., Noh, Y., & Dudhia, J. (2006). A new vertical diffusion package with an explicit treatment of entrainment processes. Mon. Wea. Rev., *134*, 2318-2341.

Juliano, T. W., Kosović, B., Jiménez, P. A., Eghdami, M., Haupt, S. E., & Martilli, A. (2022). "Gray Zone" simulations using a three-dimensional planetary boundary layer parameterization in the Weather Research and Forecasting model. Mon. Wea. Rev., *150*, 1585-1619.

Juliano, T. W., Parish, T. R., Rahn, D. A., & Leon, D. C. (2017). An atmospheric hydraulic jump in the Santa Barbara Channel. J. Appl. Meteor. Clim., *56*, 2981-2998.

Schmidli, J. (2013). Daytime heat transfer processes over mountainous terrain. J. Atmos. Sci., *70*, 4041–4066.

Smagorinsky, J. (1963). General circulation experiments with the primitive equations: I. The basic experiment. Mon. Wea. Rev., *91*, 99–164.

Wagner, J. S., Gohm, A., & Rotach, M. W. (2014). The impact of horizontal model grid resolution on the boundary layer structure over an idealized valley. Mon. Wea. Rev., *142*, 3446–3465.

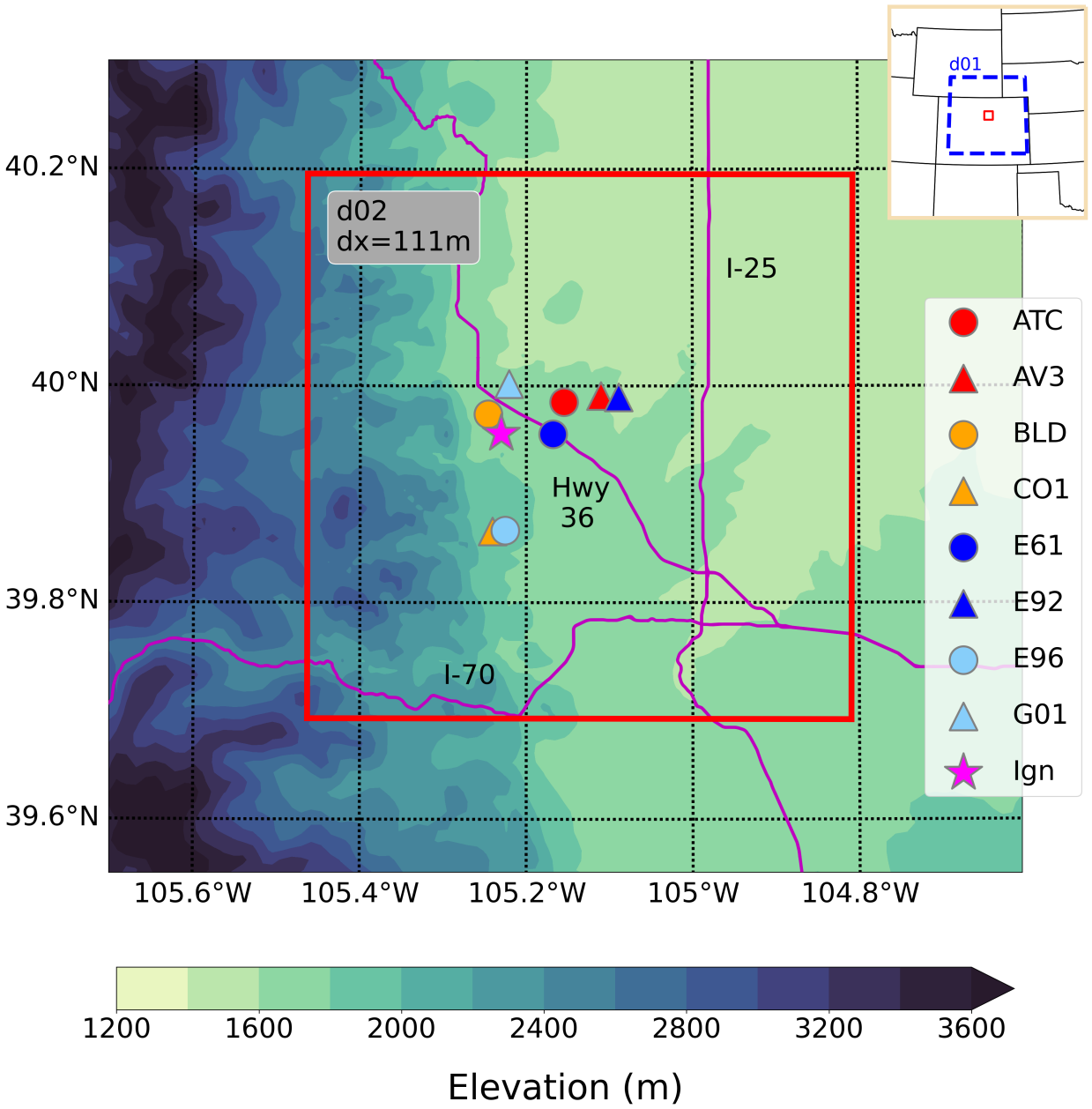

Figure S1. WRF-Fire domain configuration. The outer and inner domains are abbreviated as d01 and d02, respectively. The colored red, orange, and blue symbols represent the various surface weather stations. The magenta star represents the approximate locations of the two initial fire ignitions, which are ∼550 m apart.

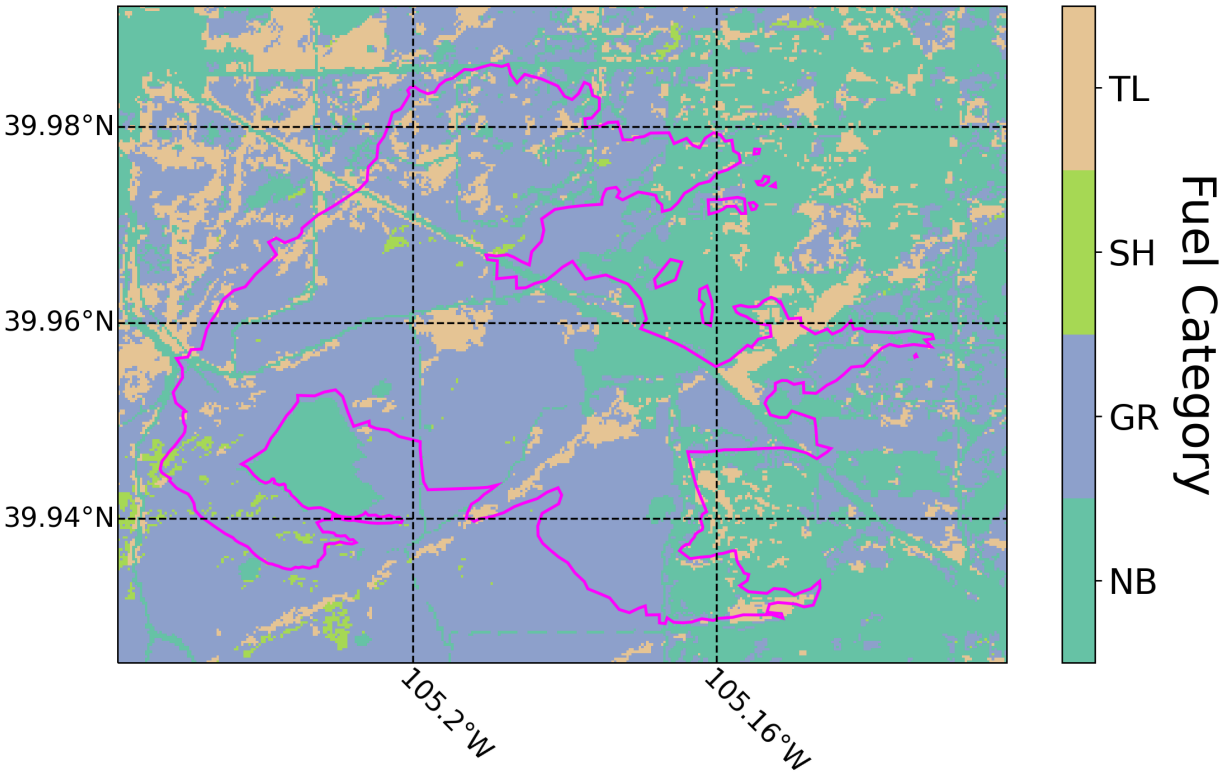

Figure S2. The Anderson 13 fuel model layers used in the WRF-Fire simulation. The final observed fire perimeter is shown in magenta. Fuel categories represent the fuel type of the fuel model;timber litter (TL), shrub (SH), grass (GR), and nonburnable (NB). Note that the slash-blowdown category is not shown due to the absence of this fuel type in our domain.

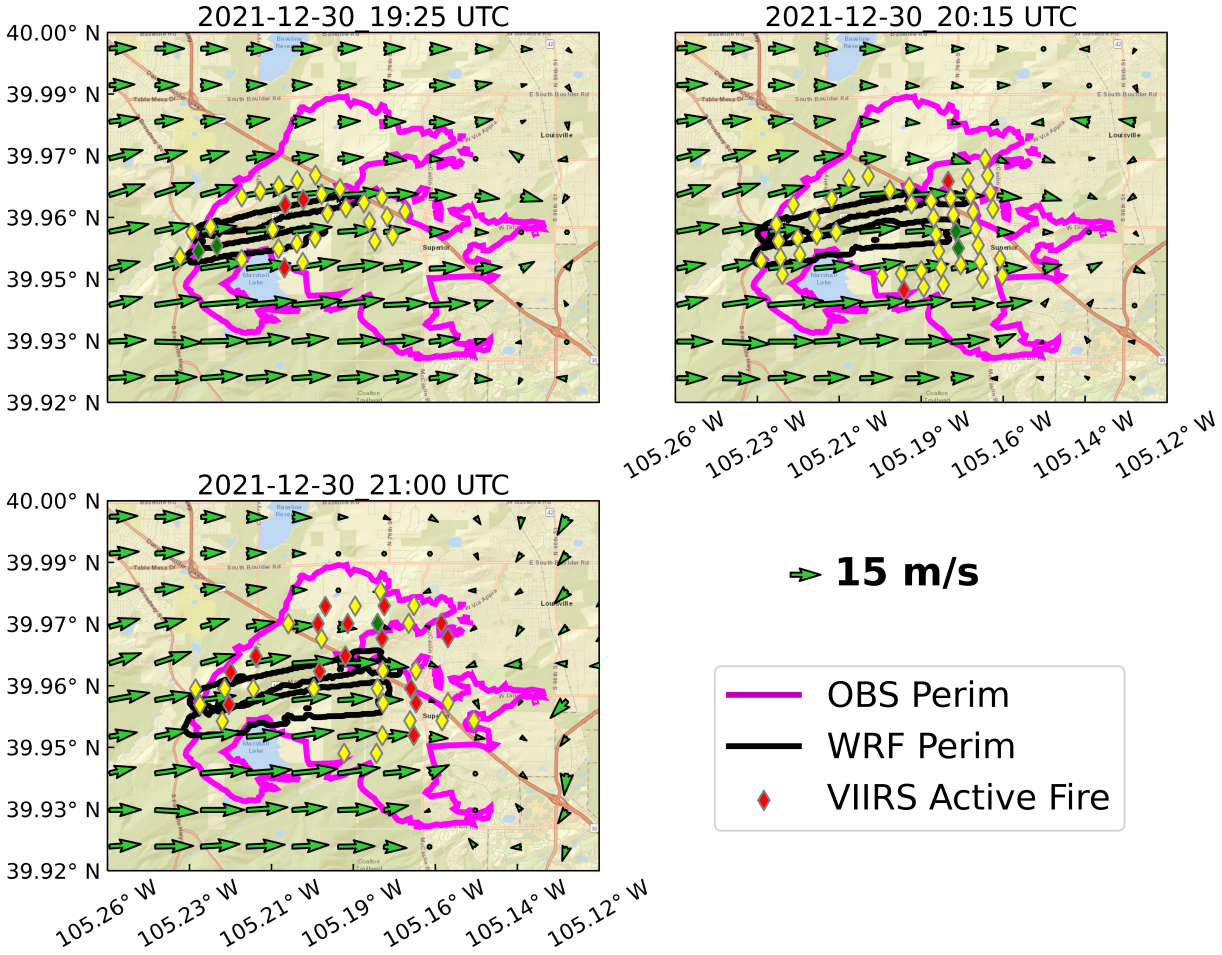

Figure S3. Temporal progression of the Marshall Fire spread. The magenta line represents the final observed perimeter and the black line represents the WRF-Fire perimeter at the indicated time. The colored diamonds represent VIIRS fire detections, with red, yellow, and green representing low, nominal, and high confidence intervals, respectively. Also shown are 10 m wind arrows with wind speed according to the key.

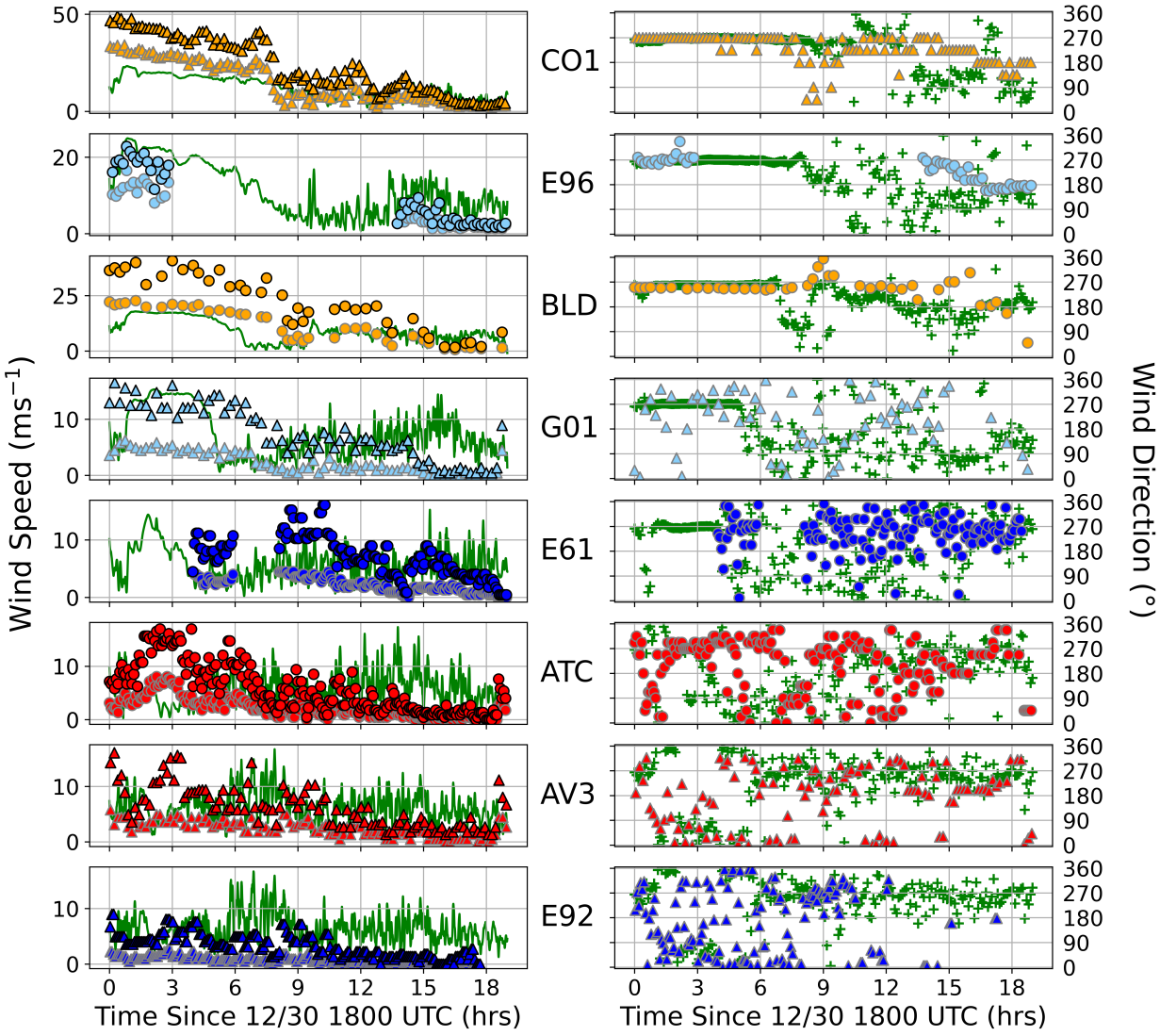

Figure S4. Time series of (left panels) wind speed and (right panels) wind direction for the various surface weather station locations. Green lines represent high-frequency ($\frac{2}{3}$ s) output from WRF, while the symbols represent observations. For the left panels, the light and dark colored symbols show the observed wind speeds and gusts, respectively.

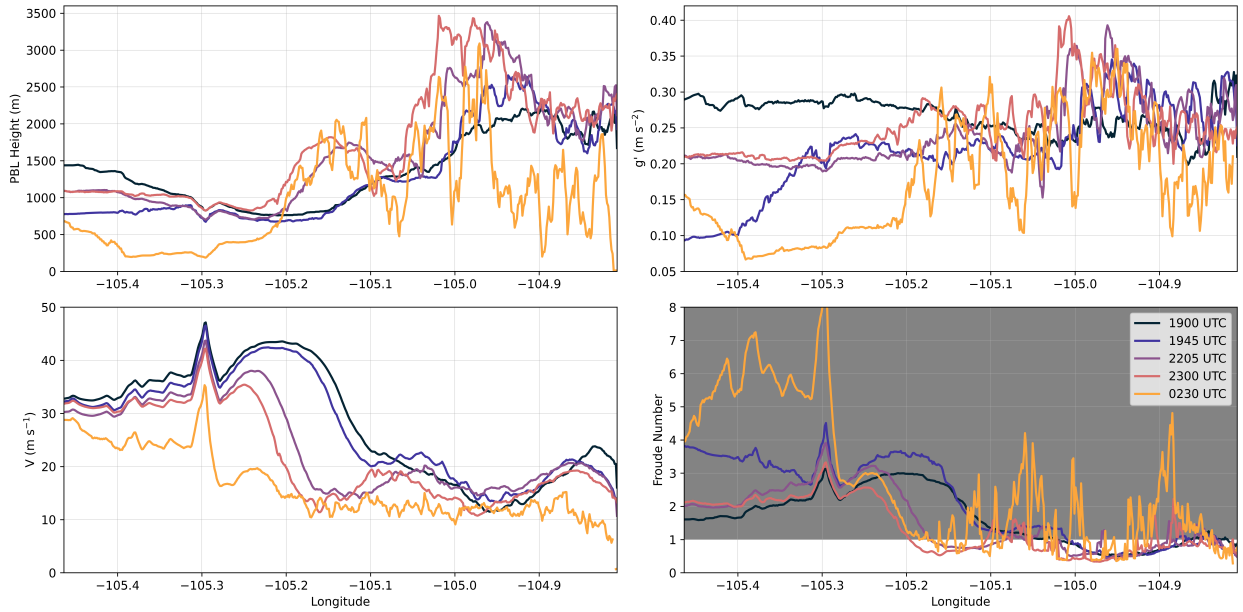

Figure S5. Fr analysis along the east-west transects in Fig. 4 showing: (top left) PBL height, (top right) reduced gravity, g$^{'}$, (bottom left) mean PBL wind speed, and (bottom right) Fr. The shaded region in the bottom right panel represents the supercritical flow region (Fr >1). Details about the Fr calculation are outlined in Text S3.

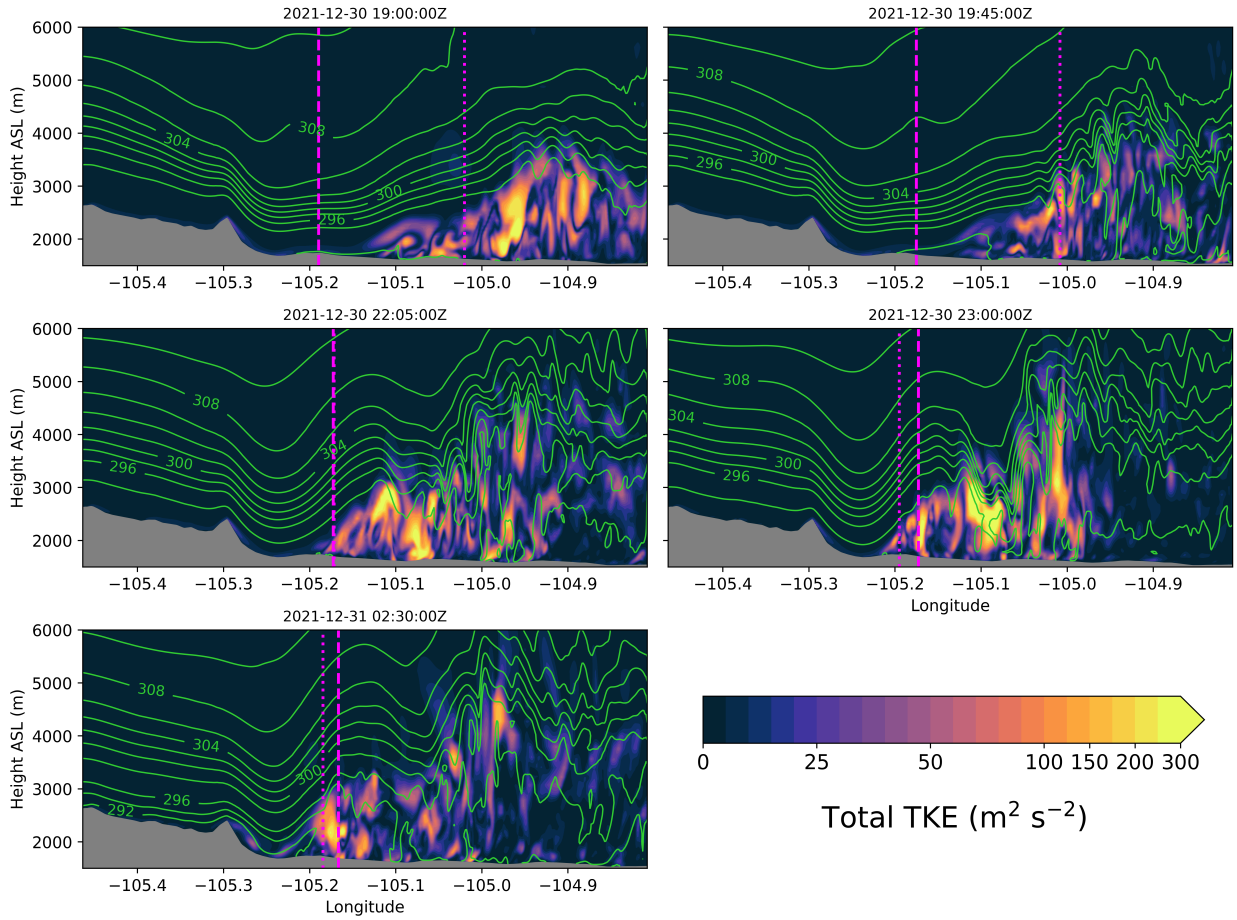

Figure S6. As in Fig. 4, except showing total (resolved plus SGS) TKE according to the colorbar. Also plotted is the location of the flow transition (Fr =1; dotted magenta line) tr Details about the TKE calculation are outlined in Text S4.

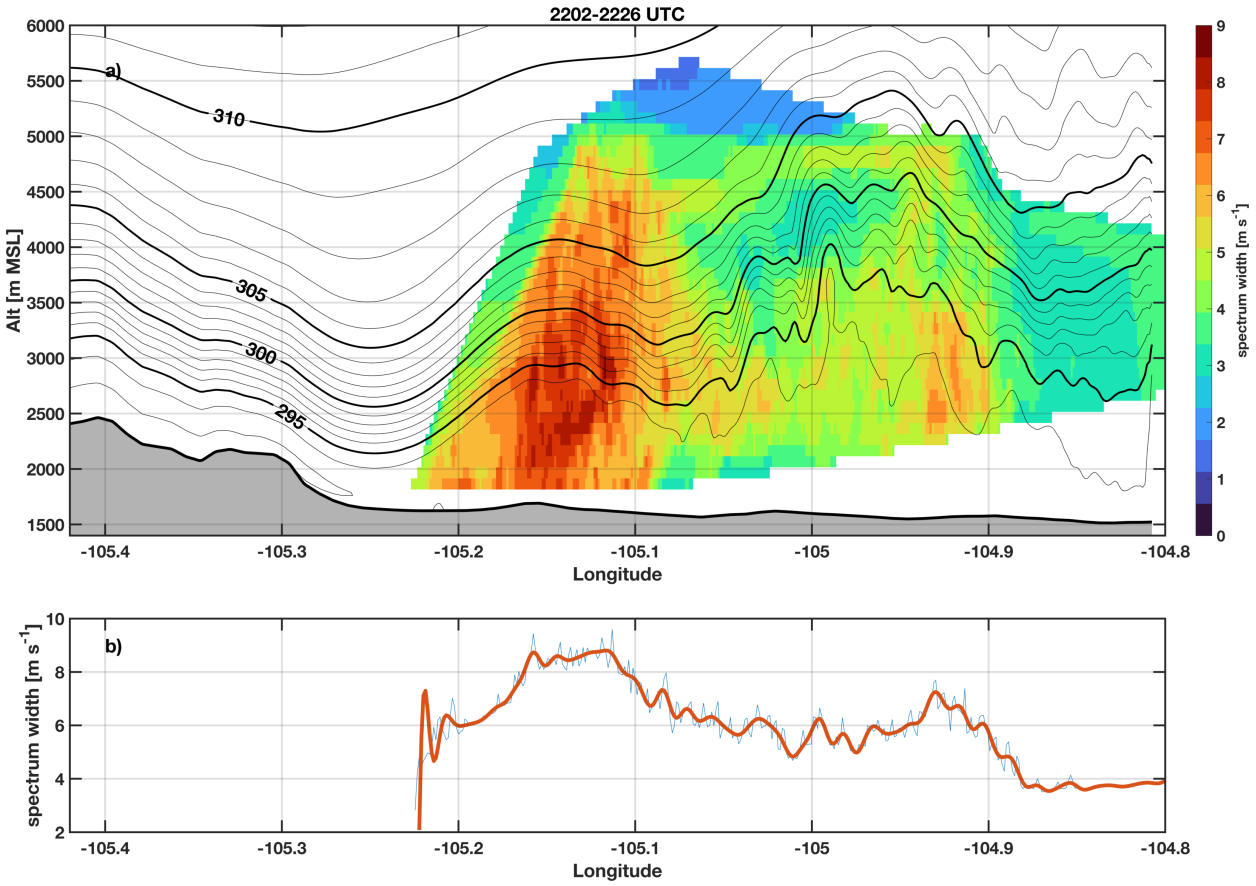

Figure S7. As in Fig. 5, except showing spectrum width.